

Article

Derivation of Relationships between Spectral Vegetation Indices from Multiple Sensors Based on Vegetation Isolines

Hiroki Yoshioka ^{1,*}, Tomoaki Miura ² and Kenta Obata ¹

¹ Department of Information Science and Technology, Aichi Prefectural University, 1522-3 Ibara, Nagakute, Aichi 480-1198, Japan; E-Mail: kenta.obata@cis.aichi-pu.ac.jp

² Department of Natural Resources and Environmental Management, University of Hawaii at Manoa, 1910 East West Road, Sherman 101, Honolulu, HI 96822, USA

* Author to whom correspondence should be addressed; E-Mail: yoshioka@ist.aichi-pu.ac.jp; Tel.: +81-561-64-1111.

Received: 31 January 2012; in revised form: 24 February 2012 / Accepted: 24 February 2012 /

Published: 28 February 2012

Abstract: An analytical form of relationship between spectral vegetation indices (VI) is derived in the context of cross calibration and translation of vegetation index products from different sensors. The derivation has been carried out based on vegetation isoline equations that relate two reflectance values observed at different wavelength ranges often represented by spectral band passes. The derivation was first introduced and explained conceptually by assuming a general functional form for VI model equation. This process is universal by which two VIs of different sensors and/or different model equations can be related conceptually. The general process was then applied to the actual case of normalized difference vegetation index (NDVI) from two sensors in a framework of inter-sensor continuity. The derivation results indicate that the NDVI from one sensor can be approximated by a rational function of NDVI from the other sensor as a parameter. Similar result was obtained for the case of soil adjusted VI, enhanced VI, and two-band variance of enhanced VI.

Keywords: data continuity; cross calibration; vegetation isoline equation; vegetation index

1. Introduction

Satellite observations play an important role for global monitoring and characterization of the atmosphere and terrestrial environment in relation with Earth system science. In these studies, multi-year to multi-decadal observation records are often required to detect changes that have occurred or are occurring, and to identify trends and causes of those changes. In order to continue long-term satellite observations effectively, an interdisciplinary approach in the framework of interagency and international cooperation is indispensable.

In the field of ocean studies, a NASA program, Sensor Intercomparison and Merger for Biological and Interdisciplinary Oceanic Studies (SIMBIOS) [1], has been operating for the integration of information from multiple satellite ocean color sensors. SIMBIOS involves extensive efforts of collection, processing, archival, and documentation of calibration datasets from multiple sensors to ultimately eliminate incompatibilities among sensor data across multiple missions [2]. For land studies, numerous efforts have been made to continue and extend the long-term dataset acquired by the Advanced Very High Resolution Radiometer (AVHRR) sensor series with current and future sensors such as Moderate Resolution Imaging Spectroradiometer (MODIS), Vegetation (VGT), Medium Resolution Imaging Spectrometer (MERIS), and Visible Infrared Imaging Radiometer Suite (VIIRS) onboard the National Polar-orbiting Operational Environmental Satellite System Preparatory Project (NPP) platform and planned for the Joint Polar Satellite System (JPSS).

Generation of such long-term observation records by merging multiple sensor data requires a considerable amount of scientific investigations on data continuity and compatibility due to differences in both hardware and software configurations, e.g., sensor/platform characteristics and processing algorithms [3–9]. Systematic differences in VI products among sensors [10] are one such problem to be resolved. Instrument spectral band-pass filters (BPFs) are one of the factors that induce systematic differences in reflectance and VIs across sensors where this paper is aimed to contribute.

Sensor calibration, including both pre- and post-launch absolute calibration and sensor cross calibrations, has been a major issue and intensively studied by numerous researchers [11–19]. In recent years, several studies were conducted to simulate broad AVHRR bands using a weighted sum of several narrow bands of new sensors for continuity and compatibility, especially, of the NDVI [20]. Gitelson and Kaufman [21] introduced a MODIS NDVI optimization method where the MODIS red-channel was adjusted by adding the MODIS green-channel with the weight optimized to fit the broader AVHRR visible channel. Gao [22] proposed a practical technique of simulating AVHRR NIR reflectance from MODIS by combining the MODIS NIR channel with the water vapor-sensitive MODIS 0.941 μm channel. A similar approach can also be seen in their earlier work [23] for the purpose of water-vapor correction in Hyperspectral data from AVIRIS known as the atmospheric removal (ATREM) program. Gunther and Maier [24] used multiple MERIS bands to simulate AVHRR red and NIR channels with the goal of deriving an AVHRR-compatible NDVI. An assumption underlying those approaches is that one sensor's output can be modeled by a weighted sum of several channels.

More recently, a modeling study was reported by Trishchenko *et al.* [10] to evaluate the effects of BPFs on surface reflectance and NDVI measured with AVHRR, MODIS, Global Imager, and Vegetation. They showed that surface reflectance and NDVI were both sensitive to the sensor's BPF across various

surface types and atmospheric conditions and concluded that the differences in surface reflectance and NDVI caused by the differences in BPFs are too large to neglect and, thus, need to be adjusted in particular for the purpose of consistent long-term monitoring of the Earth's environment by multiple satellite sensors. In their study, relationships of two NDVI values measured with different sensors were modeled by a second order polynomial.

One common aspect in the studies by Gitelson and Kaufman [21], Gao [22], and Trishchenko *et al.* [10] is that outputs from one sensor can be modeled by another with a certain functional form, *i.e.*, polynomials and weighted sums. Validity of using such functional forms which describe the relationships needs to be investigated solely from a theoretical point of view. This should also serve for better understanding of the fundamentals of multi-sensor VI continuity/compatibility.

This study is aimed at analytically providing a theoretical justification on and a functional form of inter-sensor VI relationship. In order to ensure the integrity of the derivation steps, a part of this work is devoted to provide comprehensive overview of our preliminary results [25–28]. Our approach is to use vegetation isoline equations which describe the relationships between two reflectances measured at different wavelengths for both the top-of-canopy reflectances [29,30] and the top-of-atmosphere reflectances [31]. Its applications has been reported for several purposes [32–34].

In the reminder of this paper, we first introduce our basis of VI-to-VI relationships along with a brief review of the vegetation isoline equations in Section 2. We then introduce a derivation process of a relationship between two-band VIs in a general form in Section 3. The generalized process is then extended to the case of three-band VIs in the same section. The next three sections are devoted to explain its applicability by considering actual VI models. The first case is the relationship of two NDVIs computed from two pairs of reflectance measured at different pairs of wavelength and present the derived functional form in Section 4. The derivation is further applied to the soil adjusted VI [35] and two-band enhanced VI [36] in Section 5, and finally, EVI-like model [37] as a representative of three-band VI in Section 6. Discussions and conclusions are provided in Sections 7 and 8, respectively.

2. Approach Based on Vegetation Isolines

Numerous kinds of VIs have been proposed by many researchers and routinely used for various purposes. Although those indices vary in form to some extent, the ultimate goal is to design an index sensitive only to vegetation biophysical and biochemical attributes [38] such as biomass, leaf area index (LAI), fraction of green coverage, leaf angle distribution function, fraction of absorbed photosynthetically active radiation, and leaf chemical contents. Therefore, in nature, a VI should show a strong correlation to, at least, one of these attributes. Our approach of relating two VIs also assumes such implicit, strong correlations between VIs and biophysical parameters.

From the data continuity point of view, finding NDVI-to-NDVI relationships across multiple sensors is the issue to be addressed, especially for continuation of AVHRR broader bands observations with narrower bands of new sensors. Hence, in this study, we assume the conditions that either of two VIs, for which to derive an VI-to-VI relationship, do not have a derived explicit relationship with any biophysical parameters and that the spectral band passes used to compute VIs are not identical among sensors (e.g., AVHRR channel 1 vs. MODIS band 1).

In order to derive a relationship between two VIs of different sensors under such conditions, we need to relate any two variables used in the VI model equations either implicitly (*i.e.*, about biophysical parameters) or explicitly (e.g., about reflectances). The latter approach is taken here: We relate two VIs based on the analytical relationships of two reflectances used in VI model equation. The relationships of two reflectances at different wavelengths are represented by vegetation isoline equations derived in our previous work.

The isoline equation is written by [31]

$$\rho(\lambda_2, C_v, C_a, C_s) = A(\lambda_1, \lambda_2, C_v, C_a)\rho(\lambda_1, C_v, C_a, C_s) + D(\lambda_1, \lambda_2, C_v, C_a) + O^2(\lambda_1, \lambda_2, C_v, C_a, C_s) \quad (1)$$

Since details of the isoline equation and its derivation were already provided in [31], here we explain the equation briefly. The reflectances ρ at two wavelengths, λ_1 and λ_2 , are related by the above equation as a function of biophysical parameters represented by C_v , atmospheric conditions, C_a , and soil conditions, C_s . $A(\lambda_1, \lambda_2, C_v, C_a)$ and $D(\lambda_1, \lambda_2, C_v, C_a)$ represent slope and offset of the isoline, respectively. Note that these isoline parameters are independent of the soil status, C_s , but functions of a soil line slope and offset. Thus, they are independent of the soil brightness. The last term in the isoline equation (O^2) represents the contributions of the higher order interactions between the two boundary layers, namely, the atmospheric and canopy layer, and the canopy and soil layer. As was discussed in [31], the contributions of those higher order terms are up to 5%, depending on the soil brightness and the optical thickness of the canopy layer. In this paper, for the purpose of brevity, the higher order interaction term will be implicitly included in the offset, D . The isoline equations are the key information that connects two VIs of different sensors and allows us to derive such a relationship analytically. The next section illustrates our approach in a general form. The generalized derivation is then applied to the case of NDVI-to-NDVI relationship and two other cases later in this work.

3. General Form of Inter-VI Relationships

3.1. Case of Two-Band VI

In this subsection, we introduce our derivation of inter-relating two 2-band vegetation indices in general form [25–28]. We do not specify the functional forms of the two VIs to be inter-related (v_a and v_b) and simply represent them as f_a and f_b for v_a and v_b , respectively, where subscripts a and b denote two sensors, namely sensor-a and sensor-b. Moreover the difference can be selections of VIs. For example, v_a and v_b (or f_a and f_b) can be a pair of the same VIs from different sensors (e.g., NDVI vs. NDVI), the same VIs from the same sensor but with different choices of channels (e.g., green-NIR vs. red-NIR VIs), or two different VIs from the same sensor or different sensors (NDVI vs. SAVI). The only limitation posed to this derivation is that the number of channels used for VIs is two. Assume that v_a is a function of two reflectances denoted by ρ_{a1} and ρ_{a2} ,

$$v_a = f_a(\rho_{a1}, \rho_{a2}), \quad (2)$$

and v_b is a function of ρ_{b1} and ρ_{b2} ,

$$v_b = f_b(\rho_{b1}, \rho_{b2}). \quad (3)$$

Our goal is to relate v_a and v_b with the help of vegetation isoline equations, which describe the relationship of any two reflectances. Specifically, the vegetation isoline equations are used to (1) eliminate reflectances from the VI equations and (2) relate two VIs.

The first isoline equation is introduced to relates ρ_{a1} and ρ_{a2} ,

$$\rho_{a2} = g_{a12}(\rho_{a1}). \quad (4)$$

Substituting ρ_{a2} in Equation (2), we have

$$v_a = f_a(\rho_{a1}, g_{a12}(\rho_{a1})) = f_a^*(\rho_{a1}). \quad (5)$$

Equation (5) represents the relationship between v_a and ρ_{a1} with the parameters of vegetation isolines, namely slope and offset, denoted by A and D in Equation (1), respectively.

The second isoline equation is introduced to eliminate ρ_{b2} from Equation (3). Using the same procedure taken to relate v_a and ρ_{a1} , we represent an isoline equation between ρ_{b1} and ρ_{b2} by

$$\rho_{b2} = g_{b12}(\rho_{b1}). \quad (6)$$

Substituting ρ_{b2} in Equation (3),

$$v_b = f_b(\rho_{b1}, g_{b12}(\rho_{b1})) = f_b^*(\rho_{b1}). \quad (7)$$

Solving the above equation for ρ_{b1} , we obtain

$$\rho_{b1} = f_b^{*-1}(v_b). \quad (8)$$

The last step is to relate ρ_{a1} and ρ_{b1} used in v_a and v_b , respectively, by the third isoline equation. Note that this reflectance relationship is the inter-sensor relationship that connects outputs from two sensors.

$$\rho_{a1} = g_{ba}(\rho_{b1}). \quad (9)$$

Substituting ρ_{b1} (Equation (8)) into Equation (9), we obtain

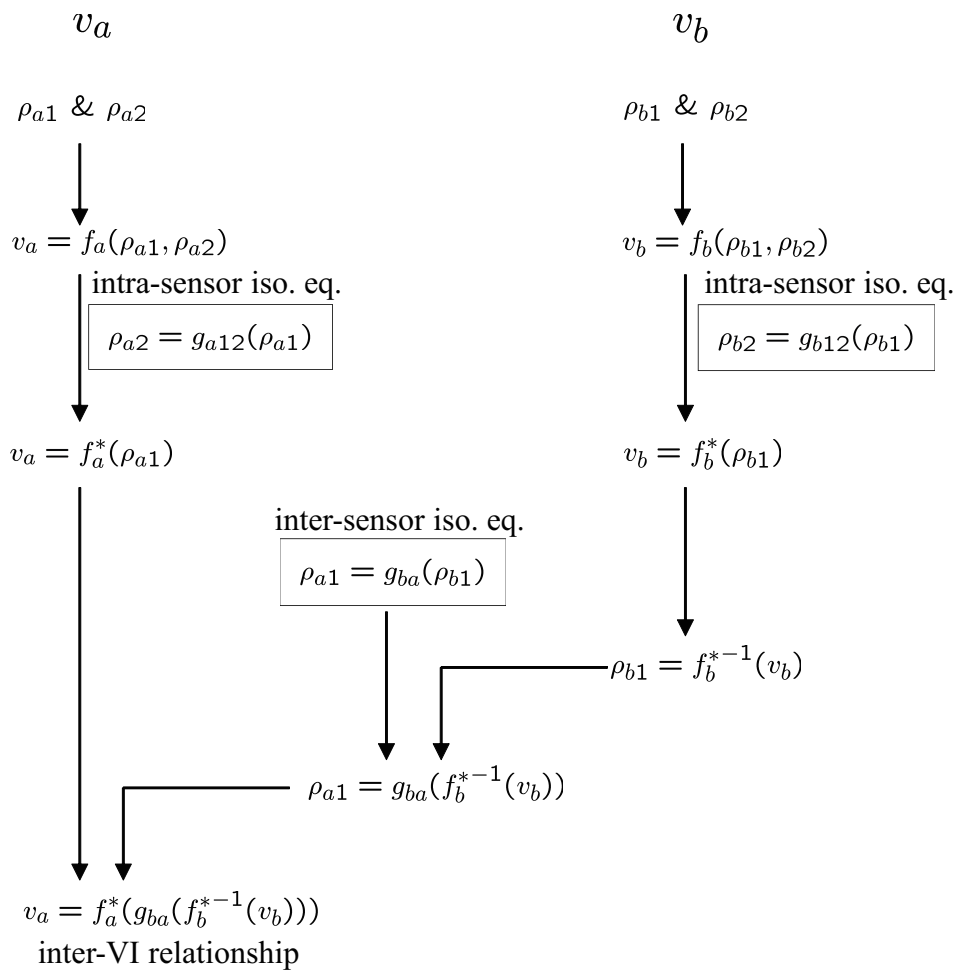
$$\rho_{a1} = g_{ba}(f_b^{*-1}(v_b)). \quad (10)$$

Finally, substituting the above expression into Equation (5), we have the relationship of v_a and v_b in the following form,

$$v_a = f_a^*(g_{ba}(f_b^{*-1}(v_b))). \quad (11)$$

Figure 1 summarizes the above derivation steps. The three isoline equations employed during the derivation are highlighted with boxes in the figure. The coefficients of g_{a12} depend only on the band characteristics of sensor-a, so they can be determined independently of sensor-b. This can be understood as a relative calibration of two channels of sensor-a (intra-sensor relative calibration). In the same manner, the coefficients of g_{b12} can be determined independently of sensor-a. The essence of inter-sensor relationship between the two sensors is then included in the function g_{ba} . This inter-sensor relative calibration of the two channels is the key information which relates two VIs. The choice of two channels could be either red channels of the two sensors, or NIR channels.

Figure 1. Illustration of the derivation steps for the case of two-band VI.



3.2. Case of Three-Band VI

The derivation steps in the previous subsection can be extended to the case of three-band VIs such as enhanced VI (EVI) [37]. The VI model is represented as a function of three reflectances of different wavelengths (bands) for both sensors. The number of unknown in this case is, thus, larger than the case of two-band VI. As a result, more number of isoline equations are needed. Specifically, two additional isoline equations are needed to eliminate the additional unknowns from the system of equations. The additional equations are an intra-sensor isoline for each sensor. The total number of isoline equations used during the derivation becomes five in the case of three-band VI.

In this case, v_a is a function of ρ_{a1} , ρ_{a2} , and ρ_{a3} ,

$$v_a = f_a(\rho_{a1}, \rho_{a2}, \rho_{a3}). \tag{12}$$

Likewise, v_b can be written as a function of ρ_{b1} , ρ_{b2} , and ρ_{b3} , represented by

$$v_b = f_b(\rho_{b1}, \rho_{b2}, \rho_{b3}). \tag{13}$$

In addition to Equation (4), we need to use the following isoline equation for sensor-a,

$$\rho_{a3} = g_{a13}(\rho_{a1}). \tag{14}$$

Substituting Equations (4) and (14) into Equation (12), we obtain

$$v_a = f_a(\rho_{a1}, g_{a12}(\rho_{a1}), g_{a13}(\rho_{a1})) = f_a^*(\rho_{a1}). \tag{15}$$

Similarly, for sensor-b, we have the following isoline equation in addition to Equation (6),

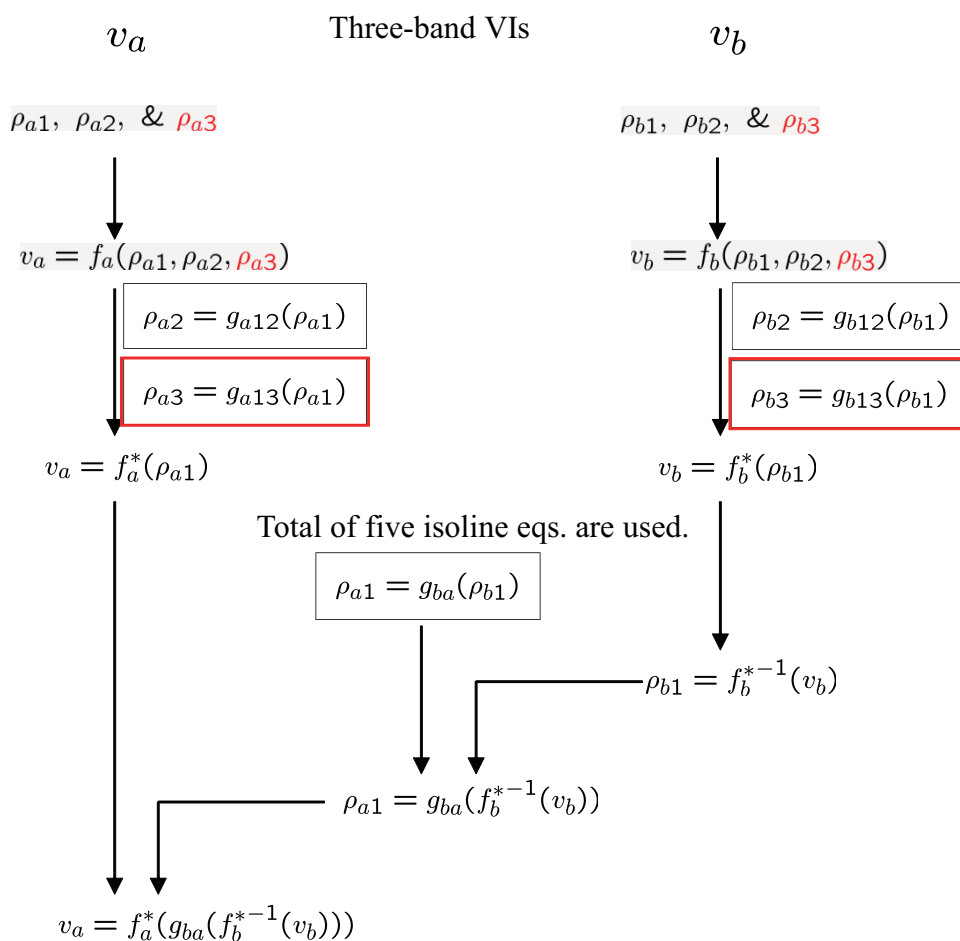
$$\rho_{b3} = g_{b13}(\rho_{b1}). \tag{16}$$

Substituting Equations (6) and (16) in Equation (13), we obtain the following expression

$$v_b = f_b(\rho_{b1}, g_{b12}(\rho_{b1}), g_{b13}(\rho_{b1})) = f_b^*(\rho_{b1}). \tag{17}$$

The remaining derivation steps are exactly the same as the case of two-band VI, which are also illustrated in Figure 2. In the figure, the differences from the case of two-band VI are highlighted by the color.

Figure 2. Illustration of the derivation steps for the case of three-band VI. The differences from the case of two-band VI are denoted by red.



4. Inter-Sensor NDVI Relationship

In this section we introduce an application of the above derivation to the case of inter-sensor NDVI relationship [25,26]. Note that, since we focus on the NDVI relationship, we assume that the reflectances

of channel-1 and -2 are employed for both sensors, which is reflected in the subscripts of the reflectances for sensor-b.

The NDVI for sensor-a, v_a , is written by

$$v_a = \frac{\rho_{a2} - \rho_{a1}}{\rho_{a2} + \rho_{a1}}. \quad (18)$$

The first isoline equation, which relates ρ_{a1} and ρ_{a2} is then denoted by,

$$\rho_{a2} = A_{a,12}\rho_{a1} + D_{a,12} = g_{a,12}(\rho_{a1}), \quad (19)$$

where $A_{a,12}$ and $D_{a,12}$ are the isoline slope and offset, respectively, for the two channels of sensor-a. Equation (19) is an analytical expression of intra-sensor vegetation isolines that can be observed in the red-NIR reflectance space.

Using Equations (18) and (19), f_a^* becomes

$$v_a = \frac{d_{a,12}^- \rho_{a1} + D_{a,12}}{d_{a,12}^+ \rho_{a1} + D_{a,12}} = f_a^*(\rho_{a1}), \quad (20)$$

where

$$d_{a,12}^\pm = A_{a,12} \pm 1. \quad (21)$$

Similarly, the NDVI observed by sensor-b, v_b , is written by ρ_{b1} and ρ_{b2} as

$$v_b = \frac{\rho_{b2} - \rho_{b1}}{\rho_{b2} + \rho_{b1}}. \quad (22)$$

By repeating the same procedure described above, ρ_{b2} is eliminated from the equation by using the second isoline equation, or the intra-sensor isoline equation between ρ_{b1} and ρ_{b2} ,

$$\rho_{b2} = A_{b,12}\rho_{b1} + D_{b,12} = g_{b,12}(\rho_{b1}), \quad (23)$$

and

$$v_b = \frac{d_{b,12}^- \rho_{b1} + D_{b,12}}{d_{b,12}^+ \rho_{b1} + D_{b,12}} = f_b^*(\rho_{b1}), \quad (24)$$

where

$$d_{b,12}^\pm = A_{b,12} \pm 1. \quad (25)$$

From the relationship between ρ_{b1} and v_b , we write ρ_{b1} in terms of v_b ,

$$\rho_{b1} = \frac{D_{b,12}(1 - v_b)}{d_{b,12}^+ v_b - d_{b,12}^-} = f_b^{*-1}(v_b). \quad (26)$$

The third isoline equation that relates ρ_{a1} and ρ_{b1} , represented by $g_{ba,1}$, is

$$\rho_{a1} = A_{ba,1}\rho_{b1} + D_{ba,1} = g_{ba,1}(\rho_{b1}). \quad (27)$$

Substituting Equation (26) into (27), we have

$$\rho_{a1} = g_{ba,1}(f_b^{*-1}(v_b)) = \frac{A_{ba,1}D_{ba,1}(1 - v_b)}{v_b d_{b,12}^+ - d_{b,12}^-} + D_{ba,1}. \quad (28)$$

From Equations (20) and (28), we obtain a relationship between v_a and v_b as

$$v_a = f_a^*(g_{ba,1}(f_b^{*-1}(v_b))) = \frac{h_1 v_b - h_2}{h_3 v_b - h_4}, \quad (29)$$

and

$$h_1 = h(d_{a,12}^-, d_{b,12}^+), \quad (30)$$

$$h_2 = h(d_{a,12}^-, d_{b,12}^-), \quad (31)$$

$$h_3 = h(d_{a,12}^+, d_{b,12}^+), \quad (32)$$

$$h_4 = h(d_{a,12}^+, d_{b,12}^-), \quad (33)$$

where

$$h(\xi, \eta) = (D_{ba,1}\xi + D_{a,12})\eta - A_{ba,1}D_{b,12}\xi. \quad (34)$$

Equation (29) is an isoline-based NDVI translation equation with the four coefficients which are actually a function of the vegetation isoline parameters in similar form. The derived translation equation indicates an important fact: its coefficients may vary with optical properties of the atmosphere and vegetation layers. Note that the derivation has been performed on the first-order approximated form of vegetation isoline (Equation (1)); a more accurate translation equation could be a ratio of higher order polynomials.

5. Inter-Sensor Relationship of SAVI/EVI2-Like Two-Band Model

In this section we extend one of our early work [26] (about the case of SAVI [35]) to the case of EVI2-like model [36]. Their VI model equations can be written in a common form as the following

$$v_a = k_3 \frac{\rho_{a2} - \rho_{a1}}{\rho_{a2} + k_1 \rho_{a1} + k_2}. \quad (35)$$

where k_i 's are the coefficients unique to each index. The derivation is proceeded on the following scaled form, instead of v_a for brevity

$$v'_a = \frac{v_a}{k_3} = \frac{\rho_{a2} - \rho_{a1}}{\rho_{a2} + k_1 \rho_{a1} + k_2}. \quad (36)$$

Using the first isoline equation (Equation (19)), v'_a becomes

$$v'_a = \frac{d_{a,12}^- \rho_{a1} + D_{a,12}}{d_{a,12}^+ \rho_{a1} + D'_{a,12}} = f_a^*(\rho_{a1}). \quad (37)$$

with the new definitions of $d_{a,12}^+$ and $D'_{a,12}$

$$d_{a,12}^+ = A_{a,12} + k_1, \quad (38)$$

and

$$D'_{a,12} = D_{a,12} + k_2. \quad (39)$$

Note that $d_{a,12}^-$ and $D_{a,12}$ remain the same (see Equations (21) and (19), respectively).

Similarly, using the second isoline equation, the rescaled VI value observed by sensor-b, v'_b , is written by

$$v'_b = \frac{d_{b,12}^- \rho_{b1} + D_{b,12}}{d_{b,12}^{'+} \rho_{b1} + D'_{b,12}} = f_b^*(\rho_{b1}) \tag{40}$$

with the definitions of $d_{b,12}^{'+}$ and $D'_{b,12}$,

$$d_{b,12}^{'+} = A_{b,12} + k_1, \tag{41}$$

and

$$D'_{b,12} = D_{b,12} + k_2. \tag{42}$$

The inter-sensor VI relationship for SAVI/EVI2-like indices is obtained from Equations (37) and (40), and the third isoline equation (Equation (27)) symbolically as

$$v'_a = f_a^*(g_{ba,1}(f_b^{*-1}(v'_b))), \tag{43}$$

and the final form becomes

$$v'_a = \frac{h_1 v'_b - h_2}{h_3 v'_b - h_4}, \tag{44}$$

or

$$v_a = k_3 \frac{h_1 v_b - k_3 h_2}{h_3 v_b - k_3 h_4}, \tag{45}$$

where

$$h_1 = (D_{ba,1} d_{a,12}^- + D_{a,12}) d_{b,12}^{'+} - A_{ba,1} D'_{b,12} d_{a,12}^-, \tag{46}$$

$$h_2 = (D_{ba,1} d_{a,12}^- + D_{a,12}) d_{b,12}^- - A_{ba,1} D_{b,12} d_{a,12}^-, \tag{47}$$

$$h_3 = (D_{ba,1} d_{a,12}^{'+} + D'_{a,12}) d_{b,12}^{'+} - A_{ba,1} D'_{b,12} d_{a,12}^{'+}, \tag{48}$$

$$h_4 = (D_{ba,1} d_{a,12}^{'+} + D'_{a,12}) d_{b,12}^- - A_{ba,1} D_{b,12} d_{a,12}^{'+}. \tag{49}$$

6. Inter-Sensor Relationship of EVI-Like Three-Band Model

In this section we further extend the derivation steps to the case of three-band VI, specifically to relate EVI-like indices from two sensors. The general form of EVI-like model can be written by

$$v_a = k_3 \frac{\rho_{a2} - \rho_{a1}}{\rho_{a2} + k_1 \rho_{a1} + k_4 \rho_{a3} + k_2}, \tag{50}$$

where k_i 's are the coefficients unique to each EVI-like model. By following the similar steps explained in the previous section, the derivation is proceeded using the scaled form, instead of v_a for brevity,

$$v'_a = \frac{v_a}{k_3} = \frac{\rho_{a2} - \rho_{a1}}{\rho_{a2} + k_1 \rho_{a1} + k_4 \rho_{a3} + k_2}. \tag{51}$$

The two intra-sensor isoline equations for sensor-a are Equations (19) and a newly defined relationship

$$\rho_{a3} = A_{a,13}\rho_{a1} + D_{a,13} = g_{a,13}(\rho_{a1}). \quad (52)$$

Using the two isoline equations, v'_a becomes

$$v'_a = \frac{d_{a,12}^-\rho_{a1} + D_{a,12}}{d_{a,123}^+\rho_{a1} + D'_{a,123}} = f_a^*(\rho_{a1}), \quad (53)$$

with the new definitions of $d_{a,123}^+$ and $D'_{a,123}$,

$$d_{a,123}^+ = A_{a,12} + k_1 + k_4 A_{a,13}, \quad (54)$$

and

$$D'_{a,123} = D_{a,12} + k_2 + k_4 D_{a,13}. \quad (55)$$

Note that $d_{a,12}^-$ and $D_{a,12}$ remain the same (see Equations (21) and (19), respectively).

Similarly, using the two intra-sensor isoline equations for sensor-b, namely Equations (23) and the following newly defined isoline

$$\rho_{b3} = A_{b,13}\rho_{b1} + D_{b,13} = g_{b,13}(\rho_{b1}), \quad (56)$$

the rescaled VI value observed by sensor-b, v'_b , is written by

$$v'_b = \frac{d_{b,12}^-\rho_{b1} + D_{b,12}}{d_{b,123}^+\rho_{b1} + D'_{b,123}} = f_b^*(\rho_{b1}) \quad (57)$$

with the definitions of $d_{b,123}^+$ and $D'_{b,123}$,

$$d_{b,123}^+ = A_{b,12} + k_1 + k_4 A_{b,13}, \quad (58)$$

and

$$D'_{b,123} = D_{b,12} + k_2 + k_4 D_{b,13}. \quad (59)$$

The inter-sensor VI relationship for EVI-like indices is obtained from Equations (53) and (57), and the inter-sensor isoline equation (Equation (27)). The final form becomes

$$v'_a = \frac{h_1 v'_b - h_2}{h_3 v'_b - h_4}, \quad (60)$$

or

$$v_a = k_3 \frac{h_1 v_b - k_3 h_2}{h_3 v_b - k_3 h_4}, \quad (61)$$

where

$$h_1 = (D_{ba,1}d_{a,12}^- + D_{a,12})d_{b,123}^+ - A_{ba,1}D'_{b,123}d_{a,12}^-, \quad (62)$$

$$h_2 = (D_{ba,1}d_{a,12}^- + D_{a,12})d_{b,12}^- - A_{ba,1}D_{b,12}d_{a,12}^-, \quad (63)$$

$$h_3 = (D_{ba,1}d_{a,123}^+ + D'_{a,123})d_{b,123}^+ - A_{ba,1}D'_{b,123}d_{a,123}^+, \quad (64)$$

$$h_4 = (D_{ba,1}d_{a,123}^+ + D'_{a,123})d_{b,12}^- - A_{ba,1}D_{b,12}d_{a,123}^+. \quad (65)$$

7. Discussion

In general, there are three factors to consider for monitoring of vegetation status with optical sensors. One factor is the sensor spatial and temporal resolutions to meet specific monitoring requirements. However, a particular choice of the spatial and temporal resolutions comes with a particular sensor with its specific spectral bandpasses. For example, MODIS is one choice for high temporal resolution monitoring while ASTER is a choice of sensor for high resolution monitoring; however, these sensors' red and NIR spectral bandpasses are different. Another factor is the index formulation (NDVI, SAVI, etc.), whether to meet required accuracy in capturing biophysical parameters of interest. The last factor is the band selection. While red and NIR spectral bands have been the most widely used combination, a green channel for example may be an alternative to the red as reported in [21].

If we limit our discussions to the spectral aspect, it is the combination of bandpasses and VI equations that characterize VI-to-VI relationships. The derivation and derived equations relating two VIs presented in this study should be applicable to many possible combinations of various bandpasses and VI equations. The reason is that the general form of relationships, Equation (11), does not assume any particular choices in the three factors (*i.e.*, sensors, VI equations, and spectral bands).

The NDVI translation equation, Equation (29), was derived as an example application of Equation (11). Equation (29) tells the relationship between two NDVIs at some constant biophysical and atmospheric condition, *i.e.*, a constant LAI value and a constant atmospheric optical thickness. This is because the h functions in the NDVI translation equation are a function of LAI and atmospheric optical thickness. If the NDVI shows a one-to-one relationship with LAI, or in other words if NDVI is free from soil influences, the h functions become a function of the NDVI and atmospheric optical thickness. If the atmosphere is constant in addition, the translation equation further reduces to be a function only of NDVI. In this case, the final form of the translation equation can be approximated as a ratio of two polynomials with NDVI (of sensor-b). However, since NDVI is influenced by the soil brightness to some extent, any translation equation that uses NDVI as the only parameter cannot eliminate variations caused by the soil brightness. From practical point of view, if one can correlate soil brightness-induced variations, the ratio of two polynomials may be one choice of the form of translation equation. The orders of these polynomials and their coefficients should be determined using actual datasets.

Our results that the h functions which determine the actual form of the translation of two VIs depend on LAI (and atmospheric conditions as well) have several important implications. First, VI-to-VI relationships change with soil brightness, biophysical, and atmospheric conditions. Even after the accurate and precise atmospheric correction, the other two parameters remain undetermined. It should be noted that the relationship derived in this work as a VI translation equation eliminates the soil brightness effect by utilizing the vegetation isoline equation. However, we still need to determine at least one more parameter, such as LAI, to minimize the variations in VI relationships. Although it is desirable to have an estimation of LAI, such an estimation is often done by using the VI itself. Moreover, the purpose of computing VI is mainly to estimate such a biophysical parameter. Therefore, it is quite reasonable to assume that LAI estimation is not available before the VI computation. As a consequence, it sounds impossible to eliminate the variance by the soil brightness. Nevertheless, there is a possibility to do so by using an independent parameter alternative to LAI. One requirement for such a parameter is using

another vegetation index than the target VI which shows stronger correlation with LAI. For example, utilizing one additional VI, the h functions could be approximated by the index. This possibility should be investigated solely.

8. Conclusions

An analytical form of relationship between spectral vegetation indices (VI) has been derived by using three of the vegetation isoline equations for the two-band case, and five isoline equations for the three-band case. The derivation steps were first introduced and explained conceptually by assuming a general functional form of VI model equation. This universal technique of the derivation with the isoline equations was then applied to the case of inter-NDVI relationship to identify functional form that is suitable to approximating the relationship. It was found that a rational function with two linear polynomials is appropriate, from analytical point of view, to approximate the relationship between the NDVIs from two sensors of different BPFs. The derivation technique was also applied to the SAVI/EVI2-like form and EVI-like three-band form of VI model equation. The derived expressions also indicate that the same functional form as the case of NDVI is relevant to model the relationships of such VIs.

Since this study clearly indicates the fact that the inter-VI relationships can be written by a rational function, one can choose such a functional form as a good candidate to model or determine the relationships, in practice, between the VIs from actual satellite data of two different sensors. In this connection, the derived expressions are useful from practical point of view. Further investigations are definitely needed to numerically demonstrate the validity of the derived expressions prior to practical applications of cross calibration of actual satellite data in the framework of continuity and compatibility studies.

Acknowledgements

This work was supported by JSPS KAKENHI 21510019 (HY) and a NASA grant NNX11AH25G (TM).

References

1. Fargion, G.S.; McClain, C.R. *SIMBIOS Project 2002 Annual Report*; Technical Report NASA Tech. Memo 2003-211 622; NASA: Greenbelt, MD, USA, 2003.
2. Kwiatkowska, E.J.; Fargion, G.S. Application of machine-learning techniques toward the creation of a consistent and calibrated global chlorophyll concentration baseline dataset using remotely sensed ocean color data. *IEEE Trans. Geosci. Remote Sens.* **2003**, *41*, 2844–2860.
3. Alberga, V. Similarity measures of remotely sensed multi-sensor images for change detection applications. *Remote Sens.* **2009**, *1*, 122–143.
4. Conrad, C.; Fritsch, S.; Zeidler, J.; Rucker, G.; Dech, S. Per-field irrigated crop classification in arid Central Asia using SPOT and ASTER data. *Remote Sens.* **2010**, *2*, 1035–1056.

5. Al-Hamdan, M.; Cruise, J.; Rickman, D.; Quattrochi, D. Effects of spatial and spectral resolutions on Fractal Dimensions in forested landscapes. *Remote Sens.* **2010**, *2*, 611–640.
6. Arai, E.; Shimabukuro, Y.E.; Pereira, G.; Vijaykumar, N.L. A multi-resolution multi-temporal technique for detecting and mapping deforestation in the Brazilian Amazon rainforest. *Remote Sens.* **2011**, *3*, 1943–1956.
7. Miller, R.L.; Liu, C.C.; Buonassissi, C.J.; Wu, A.M. A multi-sensor approach to examining the distribution of Total Suspended Matter (TSM) in the Albemarle-Pamlico Estuarine System, NC, USA. *Remote Sens.* **2011**, *3*, 962–974.
8. Gumma, M.K.; Thenkabail, P.S.; Hideto, F.; Nelson, A.; Dheeravath, V.; Busia, D.; Rala, A. Mapping irrigated areas of Ghana using Fusion of 30 m and 250 m resolution remote-sensing data. *Remote Sens.* **2011**, *3*, 816–835.
9. Dal'Asta, A.P.; Brigatti, N.; Amaral, S.; Sobral Escada, M.I.; Vieira Monteiro, A.M. Identifying spatial units of human occupation in the Brazilian Amazon using Landsat and CBERS multi-resolution imagery. *Remote Sens.* **2012**, *4*, 68–87.
10. Trishchenko, A.P.; Cihlar, J.; Li, Z. Effects of spectral response function on surface reflectance and NDVI measured with moderate resolution satellite sensors. *Remote Sens. Environ.* **2002**, *81*, 1–18.
11. Markham, B.L.; Barker, J.L. Radiometric properties of US processed Landsat MSS data. *Remote Sens. Environ.* **1987**, *22*, 39–71.
12. Price, J.C. Calibration of satellite radiometers and the comparison of vegetation indices. *Remote Sens. Environ.* **1987**, *21*, 15–27.
13. Suits, G.; Malila, W.; Weller, T. The prospects for detecting spectral shifts due to satellite sensor aging. *Remote Sens. Environ.* **1988**, *26*, 17–29.
14. Hall, F.G.; Strebel, D.E.; Nickeson, J.E.; Goetz, S.J. Radiometric rectification: Toward a common radiometric response among multirate, multisensor images. *Remote Sens. Environ.* **1991**, *35*, 11–27.
15. Che, N.; Price, J.C. Survey of radiometric calibration results and methods for visible and near infrared channels of NOAA-7, -9, and -11 AVHRRs. *Remote Sens. Environ.* **1992**, *41*, 19–27.
16. Loss, S. Calibration adjustment of the NOAA AVHRR normalized difference vegetation index without recourse to component Channel 1 and 2 data. *Int. J. Remote Sens.* **1993**, *14*, 1907–1917.
17. Kaufman, Y.J.; Holben, B.N. Calibration of the AVHRR visible and near-ir bands by atmospheric scattering, ocean glint and desert reflection. *Int. J. Remote Sens.* **1993**, *14*, 21–52.
18. Roderick, M.; Smith, R.; Lodwick, G. Calibrating long-term AVHRR-derived NDVI imagery. *Remote Sens. Environ.* **1996**, *58*, 1–12.
19. Tokola, T.; Lofman, S.; Erkkila, A. Relative calibration of multitemporal Landsat data for forest cover change detection. *Remote Sens. Environ.* **1999**, *68*, 1–11.
20. Tucker, C.J. Spectral estimation of grass canopy variables. *Remote Sens. Environ.* **1977**, *6*, 11–26.
21. Gitelson, A.A.; Kaufman, Y.J. MODIS NDVI optimization to fit the AVHRR data series-Spectral considerations. *Remote Sens. Environ.* **1998**, *66*, 343–350.
22. Gao, B. A practical method for simulating AVHRR-consistent NDVI data series using narrow MODIS channels in the 0.5–1.0 m spectral range. *IEEE Trans. Geosci. Remote Sens.* **2000**, *38*, 1969–1975.

23. Gao, B.C.; Goetz, A.F.H. Column atmospheric water vapor and vegetation liquid water retrievals from airborne imaging spectrometer data. *J. Geophys. Res.* **1990**, *95*, 3549–3564.
24. Günther, K.P.; Maier, S.W. AVHRR compatible vegetation index derived from MERIS data. *Int. J. Remote Sens.* **2007**, *28*, 693–708.
25. Yoshioka, H.; Yamamoto, H.; Miura, T. A Derivation of Relationships between Two-Band Vegetation Indices from Multiple Sensors. In *Proceedings of IEEE IGARSS'04*, Anchorage, AK, USA, 20–24 September 2004; Volume 6, pp. 3752–3754.
26. Yoshioka, H.; Miura, T.; Yamamoto, H. Relationships of Spectral Vegetation Indices for Continuity and Compatibility of Satellite Data Products. *Proc. SPIE* **2005**, *5655*, 233–240.
27. Yoshioka, H.; Miura, T.; Yamamoto, H. Analytical relationships of inter-sensor vegetation indices based on the theory of vegetation isoline. In *Proceedings of IEEE IGARSS'05*, Seoul, Korea, 25–29 July 2005; Volume 6, pp. 4164–4167.
28. Yoshioka, H.; Miura, T.; Yamamoto, H. Investigation on functional form in cross-calibration of spectral vegetation index. *Proc. SPIE* **2006**, *6298*, 629813.
29. Yoshioka, H.; Huete, A.; Miura, T. Derivation of vegetation isoline equations in red-NIR reflectance space. *IEEE Trans. Geosci. Remote Sens.* **2000**, *38*, 838–848.
30. Yoshioka, H.; Miura, T.; Huete, A.R.; Ganapol, B.D. Analysis of vegetation isolines in red-NIR reflectance space. *Remote Sens. Environ.* **2000**, *74*, 313–326.
31. Yoshioka, H. Vegetation isoline equations for an atmosphere-canopy-soil system. *IEEE Trans. Geosci. Remote Sens.* **2004**, *42*, 166–175.
32. Yoshioka, H.; Miura, T.; Huete, A.R. An isoline-based translation technique of spectral vegetation index using EO-1 Hyperion data. *IEEE Trans. Geosci. Remote Sens.* **2003**, *41*, 1363–1372.
33. Yoshioka, H.; Miura, T.; Dematte, J.A.M.; Batchily, K.; Huete, A.R. Derivation of soil line influence on two-band vegetation indices and vegetation isolines. *Remote Sens.* **2009**, *1*, 842–857.
34. Yoshioka, H.; Miura, T.; Dematte, J.A.M.; Batchily, K.; Huete, A.R. Soil line influences on two-band vegetation indices and vegetation isolines: A numerical study. *Remote Sens.* **2010**, *2*, 545–561.
35. Huete, A.R. A soil-adjusted vegetation index (SAVI). *Remote Sens. Environ.* **1988**, *25*, 295–309.
36. Jiang, Z.; Huete, A.R.; Didan, K.; Miura, T. Development of a two-band enhanced vegetation index without a blue band. *Remote Sens. Environ.* **2008**, *112*, 3833–3845.
37. Liu, H.Q.; Huete, A.R. A feedback based modification of the NDVI to minimize canopy background and atmospheric noise. *IEEE Trans. Geosci. Remote Sens.* **1995**, *33*, 457–465.
38. Verstraete, M.M.; Pinty, B. Designing optimal spectral indexes for remote sensing applications. *IEEE Trans. Geosci. Remote Sens.* **1996**, *34*, 1254–1265.